Neuroscience 286 (2015) 281–292

NADPH OXIDASE 2-DEPENDENT OXIDATIVE STRESS, MITOCHONDRIAL DAMAGE AND APOPTOSIS IN THE VENTRAL COCHLEAR NUCLEUS OF D-GALACTOSE-INDUCED AGING RATS

Z. DU,[a†] Q. YANG,[a†] L. LIU,[b] S. LI,[a] J. ZHAO,[a] J. HU,[a] C. LIU,[a] D. QIAN[a] AND C. GAO[a*]

[a] *Department of Otorhinolaryngology, Nanshan Affiliated Hospital of Guangdong Medical College, 89 Taoyuan Road, Nanshan District, Shenzhen 518052, China*

[b] *Guangxi Medical University, College of Pharmacy, Nanning 530021, China*

Abstract—Aging has been associated with oxidative stress and the accumulation of mitochondrial DNA (mtDNA) mutation. The previous study has established a mimetic rat model of aging using D-galactose (D-gal) and revealed that chronic injection of D-gal can increase NADPH oxidase (NOX)-dependent oxidative stress, mitochondrial damage and apoptosis in the peripheral auditory system. However, the effects of NOXs in the central auditory system (CAS) were still obscure. The current study was designed to investigate potential causative mechanisms of central presbycusis by using the D-gal-induced aging rats. We found that the levels of H_2O_2 and the expression of NADPH oxidase 2 (NOX2) and its corresponding subunits $P22^{phox}$, $P47^{phox}$ and $P67^{phox}$ were greatly increased in the ventral cochlear nucleus (VCN) of D-gal-treated rats as compared with controls. And, the levels of a typical biomarker of oxidative stress, 8-hydroxy-2-deoxyguanosine (8-OHdG), and the accumulation of mtDNA common deletion (CD) were also increased in the VCN of D-gal-treated rats as compared with controls. Moreover, the damage of mitochondrial ultrastructure, a decline in ATP levels, the loss of mitochondrial membrane potential (MMP), an increase in the amount of cytochrome c (cyt c) translocated to the cytoplasm and caspase-3 activation were observed in the VCN induced by D-gal. In addition, we also found that the terminal deoxynucleotidyl transferase (TdT)-mediated deoxyuridine triphosphate (dUTP) nick-end-labeling (TUNEL)-positive cells in the VCN were increased in D-gal-treated rats. Taken together, these findings suggest that NOX2-dependent oxidative stress may contribute to mitochondrial damage and activate a caspase-3-dependent apoptosis pathway in the CAS during aging. This study also provides new insights into the development of presbycusis.

Key words: age-related hearing loss, central auditory system (CAS), NADPH oxidase 2 (NOX2), oxidative damage, mitochondrial DNA common deletion (mtDNA CD), apoptosis.

INTRODUCTION

Aging is the universal physiological phenomenon occurring in living organisms that is characterized by progressive degenerative changes in many organs. Age-related hearing loss, also known as presbycusis, is thought to result from age-related degeneration of the peripheral and central components of the auditory system (Frisina and Walton, 2006; Howarth and Shone, 2006). The cochlear nucleus (CN) is the first relay station in the central auditory pathway and consists of two major divisions, the dorsal cochlear nucleus (DCN) and the ventral cochlear nucleus (VCN). They receive the output of the auditory portion of the cochlear and set up parallel analysis and perception (Frisina and Walton, 2006). According to the previous studies, although age-related degeneration of peripheral and central auditory system (CAS) is well described, the exact pathogenesis of presbycusis is largely unknown.

Oxidative stress-induced oxidative damage to various biological molecules has been proposed as important factors in the process of aging (Ozawa, 1997). In the previous study, it has been demonstrated that the NADPH oxidase 3 (NOX3) might be an important source of the reactive oxygen species (ROS) in the cochlear of D-galactose (D-gal)-induced aging rats and revealed that chronic injection of D-gal can increase NOX3-dependent oxidative stress, mitochondrial damage and apoptosis in the peripheral auditory system (PAS) (Du et al., 2012b). However, the effects of NADPH oxidases (NOXs) in the CAS were still obscure. NOXs, including NOX1, NOX2, NOX3, NOX4, NOX5, DUOX1 and DUOX2, are an important source of ROS production, NADPH oxidase 2 (NOX2) is not restricted to phagocytic cells, but it is present in a wide variety of nonphagocytic cells and tissues, including neurons (Serrano et al., 2003; Quinn et al., 2006). NOX2 and its corresponding subunits $P22^{phox}$,

*Corresponding author.
E-mail address: entcsgao@163.com (C. Gao).
† Z. Du and Q. Yang contributed equally to this work.
Abbreviations: 8-OHdG, 8-hydroxy-2-deoxyguanosine; CAS, central auditory system; CD, common deletion; cyt c, cytochrome c; DAPI, 4′,6-diamidino-2-phenylindole; D-gal, D-galactose; MDA, malondialdehyde; MMP, mitochondrial membrane potential; mtDNA, mitochondrial DNA; NOXs, NADPH oxidases; NOX2, NADPH oxidase 2; PAS, peripheral auditory system; PBS, Phosphate-buffered saline; RE, relative expression; ROS, reactive oxygen species; TBS, Tris-buffered saline; TEM, transmission electron microscopy; T-SOD, total superoxide dismutase; TUNEL, terminal deoxynucleotidyl transferase (TdT)-mediated deoxyuridine triphosphate (dUTP) nick-end-labeling; VCN, ventral cochlear nucleus.

http://dx.doi.org/10.1016/j.neuroscience.2014.11.061
0306-4522/

$P47^{phox}$ and $P67^{phox}$ form the active NOX2 enzyme complex that transports electrons from cytoplasmic NADPH to extracellular or phagosomal oxygen to generate superoxide (Bedard and Krause, 2007).

Oxidative damage to mitochondria and the accumulation of mitochondrial DNA (mtDNA) mutations are heavily implicated in the process of aging (Hamilton et al., 2001; Hiona and Leeuwenburgh, 2008). In humans, a 13-bp direct repeat (at 8470–8482 and 13,447–13,459) in the mtDNA leads to the frequent occurrence of a 4977 bp deletion (also known as the ''common deletion'', CD) by recombination between the repeats. A similar common mtDNA deletion occurs in rats due to a 16-bp direct repeat at 8103–8118 and 12,937–12,952; recombination between these repeats leads to a 4834-bp deletion. Therefore, CD has been used as a biomarker for aging (Yowe and Ames, 1998; Nicklas et al., 2004; Meissner et al., 2008; Markaryan et al., 2009). D-Gal has been used to induce oxidative stress *in vivo* to mimic natural aging in rats and the levels of mtDNA CD were significant increased in the CAS of D-gal-treated rats (Chen et al., 2010a,b; Zhong et al., 2012). However, there is no direct evidence to demonstrate that the accumulation of mtDNA CD caused by oxidative damage in the CAS of D-gal-induced aging rats.

Apoptosis may also play a key role in the age-related decline of physiological function in multiple organs (Youle and Strasser, 2008), including aging in the peripheral and central components of the auditory system (Someya et al., 2007, 2008; Chen et al., 2010a). Although the previous studies demonstrated that apoptosis cells were significantly increased in the CAS of D-gal-induced aging rats (Chen et al., 2010a,b), the cell apoptosis pathway has not been fully elucidated. In this study, we investigated the levels of H_2O_2 and the expression of NOX2 and its corresponding subunits $P22^{phox}$, $P47^{phox}$ and $P67^{phox}$, 8-hydroxy-2-deoxyguanosine (8-OHdG), cytosolic cytochrome c (cyt c) and cleaved caspase-3, the accumulation of mtDNA CD, the alteration of mitochondrial ultrastructure, the levels of ATP and mitochondrial membrane potential (MMP) and the occurrence of apoptosis in the VCN of D-gal-induced aging rats. Furthermore, we also explored the possible mechanism involved in presbycusis using D-gal-induced aging rats.

EXPERIMENTAL PROCEDURES

Animals and treatments

One hundred and seventy-six 1-month-old male Sprague–Dawley rats were obtained from the Experimental Animal Centre of the Guangxi Medical University. The rats were individually housed in a temperature-controlled (20–22 °C) room with a 12-h light–dark cycle and had free access to food and drinking water. The body weight of the experimental animals was monitored during the experiment as a general measure of health. The injection of D-gal to induce aging was administered following an established method. After acclimation for 2 weeks, the rats were randomly divided into four groups ($n = 44$ for each group) depending on the dosage of D-gal (Sigma, St. Louis, MO, USA): low, medium, high and a control group. Each day rats were injected subcutaneously with 150 mg/kg (low-dose), 300 mg/kg (medium-dose) and 500 mg/kg (high-dose) D-gal for 8 weeks; control rats were given the same volume of the vehicle (0.9% saline) for 8 weeks. After the experiment termination, the rats were anaesthetized with ketamine (30 mg/kg, i.p.) and chlorpromazine (15 mg/kg, i.m.), and blood was taken from the heart. Serum was obtained by centrifugation at 800 × *g* for 15 min at 4 °C and stored at −80 °C until the measurements of H_2O_2, total superoxide dismutase (T-SOD) activity and malondialdehyde (MDA) were performed. The VCN were dissected and used for the determination of H_2O_2 and ATP levels and the extraction of total RNA, genomic DNA, protein and mitochondria. Alternatively, they were perfused with 2.5% glutaraldehyde for morphological studies by transmission electron microscopy (TEM) or with 4% paraformaldehyde for immunohistochemical analysis and terminal deoxynucleotidyl transferase (TdT)-mediated deoxyuridine triphosphate (dUTP) nick-end-labeling (TUNEL) staining. All experiments were carried out in strict accordance with the recommendations in the Guide for the Care and Use of Laboratory Animals of the National Institutes of Health. The protocol was approved by the Committee on the Ethics of Animal Experiments of the Guangxi Medical University (Permit Number: SYXK2006-0003).

Serum H_2O_2, T-SOD activity and MDA assay

Using the serum from forty-eight rats ($n = 12$ per group), the H_2O_2, T-SOD activity and MDA were quantified using colorimetric kits (Jiancheng, Nanjing, China) according to the manufacturer's instructions.

Tissue H_2O_2 assay

After the last injection, twenty-four rats ($n = 6$ per group) were killed, and both sides of VCN from each rat were rapidly removed and homogenized in cold saline. The homogenate was centrifuged at 4000 × *g* for 15 min at 4 °C, and the supernatant was used for H_2O_2 assay. Protein concentrations were determined using an Enhanced BCA Protein Assay Kit (Beyotime, Haimen, China). H_2O_2 in the VCN was quantified using colorimetric kits (Jiancheng, Nanjing, China) according to the manufacturer's instructions.

RNA preparation and quantitative real-time polymerase chain reaction (RT-PCR)

The mRNA expression levels of NOX2, $p22^{phox}$, $p47^{phox}$ and $p67^{phox}$ were determined by quantitative real-time SYBR Green PCR. After the last injection, twenty-four rats ($n = 6$ per group) were killed, and both sides of VCN from each rat were rapidly removed. One side of the VCN was used for RNA extraction, and the other side of the VCN was used for mtDNA analysis (see below). Total RNA was extracted with TRIzol reagent (TaKaRa, Dalian, China) according to the manufacturer's protocol. cDNA was reverse transcribed using a PrimeScript RT reagent Kit (TaKaRa, Dalian,

Table 1. The nucleotide sequences of the primers that were used in real-time

Gene	Sequence (5′–3′)		Product size (bp)
NOX2	Forward	ACATTTTCGTCAAGCGTCCC	260
	Reverse	CCCAGCTCCCACTAACATCA	
$P22^{phox}$	Forward	ACCGTCTGCTTGGCCATTG	74
	Reverse	TCAATGGGAGTCCACTGCTCAC	
$P47^{phox}$	Forward	GAGACATACCTGACGGCCAAAGA	91
	Reverse	AGTCAGCGATGGCCCGATAG	
$P67^{phox}$	Forward	GGACAACAGAGCCTCAGCCTAA	143
	Reverse	CCCTTCCAGCCATTCTTCATTCAC	
β-Actin	Forward	CCTGGAGAAGAGCTATGAGC	112
	Reverse	ACAGGATTCCATACCCAGG	

China). The RNA and cDNA of each sample were analyzed using a GeneQuant pro DNA/RNA Calculator to assess the concentrations and purity. The cDNA samples were stored at −20 °C until use. Quantitative real-time PCR was performed by applying the real-time SYBR Green PCR technology with the use of a StepOnePlus™ Real-time PCR System (Applied Biosystems, Foster City, CA, USA). The primer pairs for NOX2, $P22^{phox}$, $P47^{phox}$, $P67^{phox}$ and an internal standard (β-actin) were listed in Table 1. The amplification conditions were as follows: 30 s at 95 °C, and then 40 cycles of 5 s at 95 °C, 30 s at 60 °C, and 30 s at 72 °C. An internal standard was used to normalize the relative gene expression levels. A melting curve analysis was performed for each gene, and the specificity and integrity of the PCR products were confirmed by the presence of a single peak. The relative expressions (REs) were calculated from the differences in the Ct values between the target mRNA and an internal standard (β-actin). The change in the relative mRNA levels between the experimental group and the control group was analyzed by using the $2^{-\Delta\Delta Ct}$ method, as previously reported (Livak and Schmittgen, 2001).

Immunohistochemical analysis

The protein levels of NOX2 and 8-OHdG, a biomarker of DNA oxidative damage (Kujoth et al., 2005; Ma et al., 2011), were determined by immunohistochemistry. Sixteen rats (n = 4 per group) were killed, and brains were fixed with 4% buffered paraformaldehyde overnight, dehydrated, and embedded in paraffin wax. Subsequently, serial sections of the brainstem were cut for 5-μm thick at the level of the VCN. The VCN from one side was used for immunohistochemical analysis, and the other side VCN was used for TUNEL assay. A section was deparaffinized in xylene and rehydrated through graded concentrations of ethanol. Samples were incubated with an anti-NOX2 antibody (diluted 1:200; Boster, Wuhan, China) and anti-8-OHdG antibody (diluted 1:4000, Abcam, Cambridge, MA, USA) overnight at 4 °C. After washes in phosphate-buffered saline (PBS), slides were then incubated with fluorescein isothiocyanate (FITC)-conjugated anti-rabbit and CY3-conjugated anti-mouse secondary antibody (diluted 1:200; Boster, Wuhan, China) for 30 min at room temperature. Nuclei were counterstained with a 4′,6-diamidino-2-phenylindole (DAPI) staining solution (Beyotime, Haimen, China) for 5 min at room temperature. Images were captured using a laser scanning confocal microscope (Nikon, Tokyo, Japan). The number of NOX2-positive and 8-OHdG-positive stained cells were counted using the Image-Pro Plus 6.0 software (Media Cybernetics, Inc., Silver Spring, MD, USA). As a negative control, sections were treated in the same manner, except that incubation with primary antibody was omitted.

Western blot analysis

The protein expression levels of $p22^{phox}$, $p47^{phox}$, $p67^{phox}$, cleaved caspase-3 and cytosolic cyt c in the VCN were determined using Western blot analysis. Fourty-eight rats (n = 12 per group) were killed, and the both sides of VCN from each rat were dissected. Preparation of cytosolic fractions was achieved using a commercially available cytosol/mitochondria fractionation Kit (Beyotime, China) according to the manufacturer's protocol. Total protein and cytosolic protein were extracted using a RIPA Lysis Buffer (Beyotime, China) following the manufacturer's instructions. Protein concentrations were determined using an Enhanced BCA Protein Assay Kit (Beyotime, Haimen, China). Twenty-five micrograms of each protein lysate was separated by 10% ($p22^{phox}$, $p47^{phox}$, $p67^{phox}$, cleaved caspase-3) or 12% (cytosolic cyt c) sodium dodecyl sulfate (SDS)–polyacrylamide gels and transferred to polyvinylidene difluoride (PVDF) membranes. Membranes were incubated for 1 h in a blocking solution (Tris-buffered saline (TBS) containing 5% skimmed milk), then washed briefly in TBS and incubated overnight at 4 °C with the appropriate dilution of antibodies: anti-$p22^{phox}$ (diluted 1:100; Boster, China), anti-$p47^{phox}$ (diluted 1:500; Bioworld Technology, Inc., Louis Park, MN, USA), anti-$p67^{phox}$ (diluted 1:1000, Epitomics, Inc., Burlingame, CA, USA), anti-cleaved caspase-3 (diluted 1:1000; Cell Signaling Technology, Inc., Beverly, MA, USA), anti-cyt c (diluted 1:200; Santa Cruz, Santa Cruz, CA, USA). After washing the membranes to remove excess primary antibody, the membranes were incubated for 1 h at room temperature with the appropriate horseradish peroxidase (HRP)-conjugated secondary antibody (diluted 1:5000; Santa Cruz, Santa Cruz, CA, USA). Membranes were

visualized using BeyoECL Plus (Beyotime, Haimen, China). A quantitation of the detected bands was performed with the Image-Pro Plus 6.0 software (Media Cybernetics, Inc., Silver Spring, MD, USA). β-Actin was used as an internal control.

DNA isolation and determination of the mtDNA CD

Total DNA was extracted using the Genomic DNA Purification Kit (Tiangen Biotech Co., LTD, Beijing, China) according to the manufacturer's instructions. The DNA concentration of each specimen was measured using the GeneQuant pro DNA/RNA Calculator (BioChrom, Cambridge, UK). The quantity of the mtDNA CD was determined using a TaqMan real-time PCR assay. Because the D-Loop region is rarely deleted, it can represent the conserved segment. Primers and probes for the mtDNA D-loop and the mtDNA CD were previously described (Nicklas et al., 2004). The PCR amplification was performed on a StepOnePlus™ Real-time PCR System (Applied Biosystems, Foster City, CA, USA) in a 20-μl reaction volume consisting of 10 μl of a 2× TaqMan PCR mix (TaKaRa, Dalian, China), 0.4 μl of a 50× ROX reference dye, 0.4 μl of each forward and reverse primer (10 μM), 0.2 μl of each probe (10 μM), 4 μl of the sample DNA (10 ng/μl), and 4.6 μl of distilled water. The cycling conditions include an initial phase at 95 °C for 30 s, then 40 cycles at 95 °C for 5 s and at 60 °C for 30 s. The cycle number at which a significant increase in the normalized fluorescence was first detected was designated as the threshold cycle number (Ct). The ratio of the mtDNA CD to the mtDNA was calculated by ΔCt ($= Ct_{\text{mtDNA deletion}} - Ct_{\text{mtDNA D-loop}}$). The RE indicates the factorial difference in the deletions between the experimental groups and the control group. The RE was calculated as $2^{-\Delta\Delta Ct}$, where $\Delta\Delta Ct = \Delta Ct_{\text{mtDNA deletion in experimental group}} - \Delta Ct_{\text{mtDNA deletion in the control group}}$.

TEM

The ultrastructure of mitochondria in the VCN was observed by TEM. Sixteen rats ($n = 4$ per group) were sacrificed, and both sides of VCN from each rat were fixed and perfused with 2.5% glutaraldehyde overnight at 4 °C. After post-fixation in 1% osmium tetroxide for 2 h at room temperature, the tissues were dehydrated in an ascending graded ethanol and acetone series, immersed in an acetone/Epon 812 mixture for 2 h and then in Epon 812 for 2 h, and finally embedded in Epon 812 for 10 h at 80 °C. Serial ultrathin sections (50 nm) were collected onto copper grids and stained with uranyl acetate followed by lead citrate. The ultrastructure of the stained sections was examined under a transmission electron microscope (FEI TecnaiG^{2}12, Phillips, Holland).

Detection of ATP levels

After the last injection, twenty-four rats ($n = 6$ per group) were killed, and both sides of the VCN from each rat were rapidly removed and homogenized in cold saline. The homogenized was centrifuged at 4000 × g for 15 min at 4 °C, and the supernatant was used for ATP detection. Protein concentrations were determined using an Enhanced BCA Protein Assay Kit (Beyotime, Haimen, China). ATP in the VCN was quantified using colorimetric kits (Jiancheng, Nanjing, China) according to the manufacturer's instructions.

Measurement of MMP

After the last injection, twenty-four rats ($n = 6$ per group) were killed, and both sides of the VCN from each rat were rapidly removed. Mitochondria in the VCN were quickly extracted using Tissue Mitochondria Isolation Kit (Beyotime, Haimen, China), and then used for the measurement of MMP. MMP in the VCN was quantified using the fluorescent, lipophilic and cationic probe, JC-1 (Jiancheng, Nanjing, China) according to the manufacturer's instructions.

TUNEL assay

Apoptotic cells were detected *in situ* using the TUNEL assay (TUNEL POD kit; Roche Molecular Biochemicals, Germany). Briefly, a section was deparaffinized and rehydrated. After treatment with proteinase K (20 μg/ml in 10 mM Tris–HCl, pH 7.6) for 10 min at 37 °C, sections were washed in PBS, and the labeling reaction was performed using a labeling solution containing terminal deoxynucleotidyl transferase, its buffer, and fluorescein deoxyuridine triphosphate (dUTP) at 37 °C for 60 min in a humidity chamber. Nuclei were counterstained with a DAPI staining solution (Beyotime, Haimen, China) for 5 min at room temperature. After washing with PBS, sections were examined under a laser scanning confocal microscope (Nikon, Tokyo, Japan).

Statistical analysis

Data are presented as mean ± standard deviation (SD). The analysis was performed with the SPSS 13.0 software (SPSS Inc., Chicago, IL, USA). Statistical significance was tested with a one-way analysis of variance (ANOVA). The least significant difference post hoc test was used to evaluate the differences between groups. Differences with a P-value < 0.05 were considered to be statistically significant.

RESULTS

Oxidative stress in the blood induced by D-gal

To evaluate oxidative stress induced by D-gal in this model, the serum H_2O_2, T-SOD activity and MDA levels were measured. The levels of serum H_2O_2 in the low-dose, medium-dose and high-dose groups of D-gal-treated rats were 17.04 ± 2.07 μmol/ml, 19.47 ± 2.66 μmol/ml, 25.89 ± 2.15 μmol/ml, respectively, which were significantly higher than those in the control group (12.31 ± 2.28 μmol/ml) ($P < 0.01$); Levels of serum MDA in the low-dose, medium-dose and high-dose groups of D-gal-treated rats were 5.12 ± 0.95 nmol/ml, 6.48 ± 1.04 nmol/ml, 8.23 ± 1.05 nmol/ml, respectively, which were significantly higher than those in the control group (3.23 ± 0.78 nmol/ml) ($P < 0.01$); Levels

Table 2. Serum H_2O_2, T-SOD activity and MDA levels

	Control	D-Gal (L)	D-Gal (M)	D-Gal (H)
H_2O_2 (μmol/ml)	12.31 ± 2.28	17.04 ± 2.07**	19.47 ± 2.66**	25.89 ± 2.15**
T-SOD (U/ml)	126.02 ± 6.93	114.13 ± 5.61**	96.16 ± 7.77**	74.30 ± 5.82**
MDA (nmol/ml)	3.23 ± 0.78	5.12 ± 0.95**	6.48 ± 1.04**	8.23 ± 1.05**

Data are expressed as mean ± SD of 12 rats per group. $^{**}P < 0.01$ versus the control group. MDA, malondialdehyde; T-SOD, total superoxide dismutase. D-gal (L), low-dose D-gal group; D-gal (M), medium-dose D-gal group; D-gal (H), high-dose D-gal group.

of T-SOD in the low-dose, medium-dose and high-dose groups of D-gal-treated rats were 114.13 ± 5.61 U/ml, 96.16 ± 7.77 U/ml, 74.30 ± 5.82 U/ml, respectively, which were significantly lower than those in the control group (126.02 ± 6.93 U/ml) ($P < 0.01$) (Table 2). These findings indicated that we could establish the animal model of mimetic aging by D-gal.

Increased H_2O_2 levels in the VCN induced by D-gal

To investigate the generation of ROS in the VCN, we detected the levels of H_2O_2. As shown in Fig. 1, the levels of H_2O_2 in the low-dose, medium-dose and high-dose groups of D-gal-treated rats were 20.93 ± 0.82 mmol/g protein, 26.54 ± 0.65 mmol/g protein, 34.35 ± 0.63 mmol/g protein, respectively, which were significantly higher than those in the control group (15.31 ± 0.67 mmol/g protein) ($P < 0.01$). These findings indicated that oxidative stress was induced by D-gal in the VCN.

Increased mRNA levels of NOX2, $p22^{phox}$, $p47^{phox}$ and $p67^{phox}$ in the VCN induced by D-gal

To investigate the effect of NOX2-dependent oxidative stress induced by D-gal in the VCN, we measured the mRNA levels of NOX2, $p22^{phox}$, $p47^{phox}$ and $p67^{phox}$ with a quantitative real-time SYBR Green PCR assay. As shown in Fig. 2, the mRNA levels of NOX2, $p22^{phox}$, $p47^{phox}$ and $p67^{phox}$ were significantly higher in the D-gal-treated groups than that in the control group. In comparison with the control group, NOX2 expression in the low-dose, medium-dose and high-dose D-gal groups

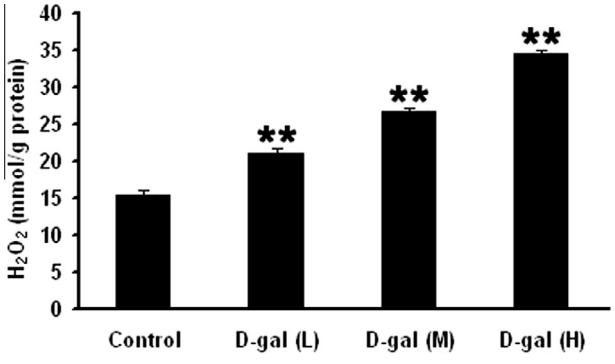

Fig. 1. Levels of H_2O_2 in the VCN of rats in the different groups. Levels of H_2O_2 in the VCN were significantly increased in D-gal-treated rats as compared with control rats. All experiments were repeated three times. Data are expressed as mean ± SD of six rats per group. $^{**}P < 0.01$ versus the control group. D-gal (L), low-dose D-gal group; D-gal (M), medium-dose D-gal group; D-gal (H), high-dose D-gal group.

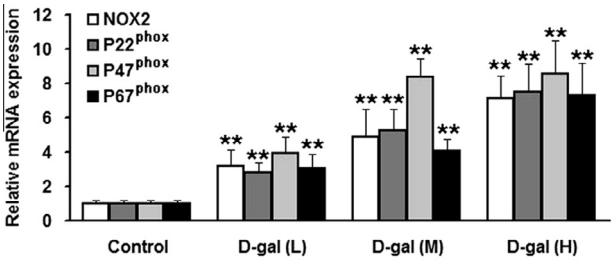

Fig. 2. Quantitative analysis of NOX2, $p22^{phox}$, $p47^{phox}$ and $p67^{phox}$ in the VCN of rats in the different groups. The expression levels of NOX2, $p22^{phox}$, $p47^{phox}$ and $p67^{phox}$ were significantly increased in D-gal-treated rats as compared with control rats. All experiments were repeated three times. Data are expressed as mean ± SD of six rats per group. $^{**}P < 0.01$ versus the control group. D-gal (L), low-dose D-gal group; D-gal (M), medium-dose D-gal group; D-gal (H), high-dose D-gal group.

was increased by 3.17-fold, 4.85-fold, 7.14-fold, respectively ($P < 0.01$); $p22^{phox}$ expression in the low-dose, medium-dose and high-dose D-gal groups was increased by 2.81-fold, 5.27-fold, 7.48-fold, respectively ($P < 0.01$); $p47^{phox}$ expression in the low-dose, medium-dose and high-dose D-gal groups was increased by 3.97-fold, 8.37-fold, 8.58-fold, respectively ($P < 0.01$); $p67^{phox}$ expression in the low-dose, medium-dose and high-dose D-gal groups was increased by 3.06-fold, 4.09-fold, 7.34-fold, respectively ($P < 0.01$). These findings indicated that the over-expression of NOX2 may be the source of ROS in the VCN of D-gal-induced aging rats.

Increased protein levels of NOX2 and 8-OHdG expression in the VCN induced by D-gal

To investigate the protein levels of NOX2 and 8-OHdG expression in the VCN, we performed an immunohistochemical analysis. As shown in Fig. 3A, B, the NOX2-positive cells in the low-dose, medium-dose and high-dose groups of D-gal-treated rats were 12.72 ± 2.21, 26.33 ± 4.50, 56.91 ± 7.62, respectively, which were significantly increased compared with those in the control group (5.82 ± 1.31) ($P < 0.01$); the 8-OHdG-positive cells in the low-dose, medium-dose and high-dose groups of D-gal-treated rats were 9.13 ± 1.81, 18.42 ± 3.23, 43.31 ± 5.84, respectively, which were significantly increased compared with those in the control group (5.20 ± 0.73) ($P < 0.01$). Moreover, we noticed that almost all the NOX2-positve cells are also 8-OHdG-positive in the VCN (Fig. 3A). These findings further indicated that the over-expression of NOX2 may be the source of ROS and NOX2-dependent

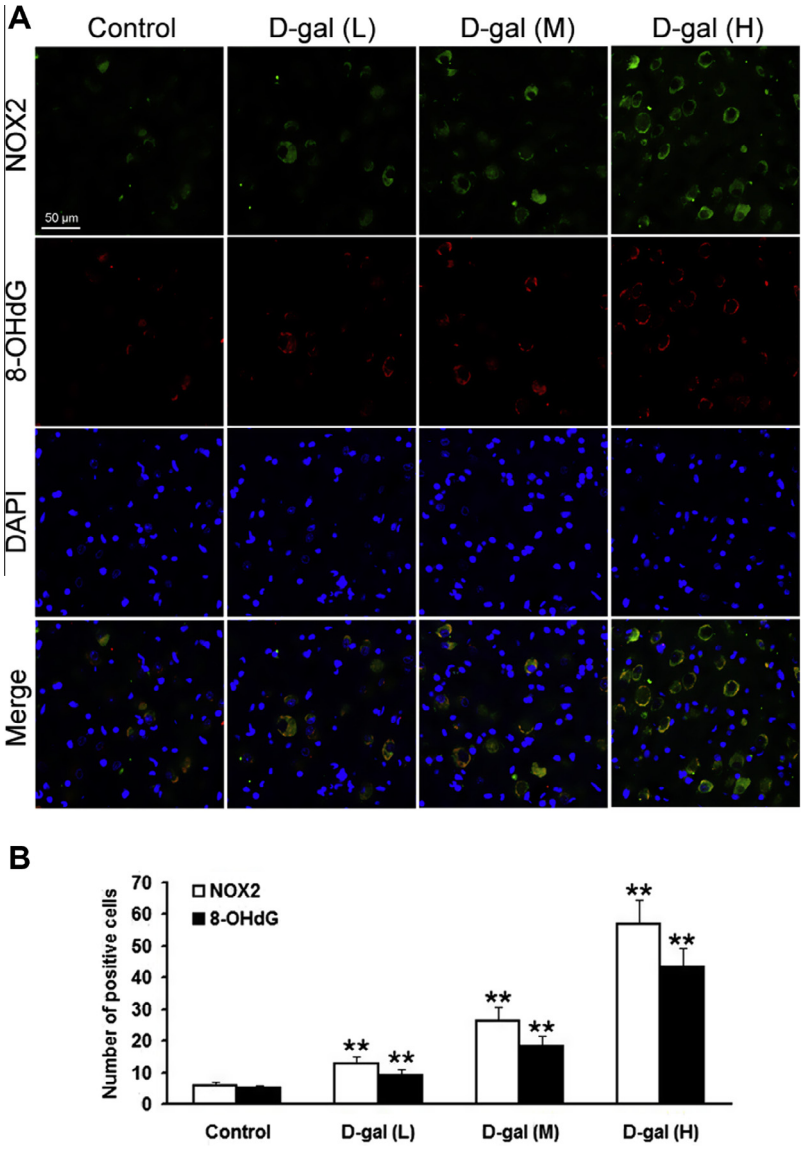

Fig. 3. The protein expression of NOX2 and 8-OHdG in the VCN of rats in the different groups. (A) Triple staining of the brain section with anti-NOX2 (green), anti-8-OHdG (red) and the nuclei of cells (blue). Note that almost all the NOX2-positve cells are also 8-OHdG-positive in the VCN. Scalar bar = 50 μm. (B) Quantitative assessment of NOX2- and 8-OHdG-positive cells in the VCN. The NOX2- and 8-OHdG-positive cells in the VCN were significantly increased in D-gal-treated rats as compared with control rats. All experiments were repeated three times. Data are expressed as mean ± SD of four rats per group. $^{**}P < 0.01$ versus the control group. D-gal (L), low-dose D-gal group; D-gal (M), medium-dose D-gal group; D-gal (H), high-dose D-gal group. (For interpretation of the references to color in this figure legend, the reader is referred to the web version of this article.)

oxidative stress may cause DNA damage in the VCN of D-gal-induced aging rats.

Increased protein levels of $p22^{phox}$, $p47^{phox}$ and $p67^{phox}$ in the VCN induced by D-gal

To determine the protein levels of $p22^{phox}$, $p47^{phox}$ and $p67^{phox}$ in the VCN, western blot analysis was performed. As shown in Fig. 4A, B, the protein levels of $p22^{phox}$, $p47^{phox}$ and $p67^{phox}$ were significantly higher in the D-gal-treated groups than that in the control group. In comparison with the control group, $p22^{phox}$ protein expression in the low-dose, medium-dose and high-dose D-gal groups was increased by 3.15-fold, 4.98-fold, 7.56-fold, respectively ($P < 0.01$); $p47^{phox}$ protein expression in the low-dose, medium-dose and high-dose D-gal groups was increased by 4.24-fold, 8.27-fold, 8.68-fold, respectively ($P < 0.01$); $p67^{phox}$ protein expression in the low-dose, medium-dose and high-dose D-gal groups was increased by 3.62-fold, 5.23-fold, 7.22-fold, respectively ($P < 0.01$). These findings further indicated that the over-expression of NOX2 may be the source of ROS in the VCN of D-gal-induced aging rats.

Age-related accumulation of the mtDNA CD in the VCN induced by D-gal

To evaluate the mtDNA damage induced by D-gal in the VCN, the mtDNA CD was determined by a TaqMan real-time PCR assay. The dual-labeled fluorescent DNA

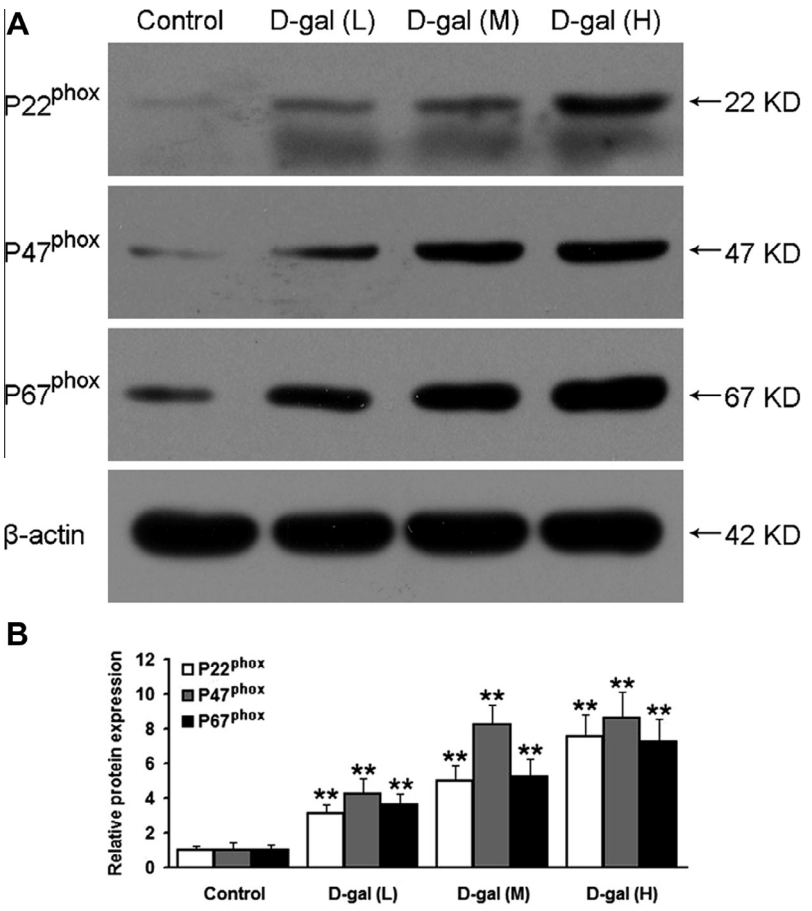

Fig. 4. Western blot and densitometric analysis of $p22^{phox}$, $p47^{phox}$ and $p67^{phox}$ in the VCN. (A) Representative western blots showing the expression levels of $p22^{phox}$, $p47^{phox}$ and $p67^{phox}$ in the different groups. (B) The relative abundances of the $p22^{phox}$, $p47^{phox}$ and $p67^{phox}$ proteins were significantly increased in the D-gal-treated groups compared to the control group. All experiments were repeated three times. Data are expressed as mean ± SD of six rats per group. $^{**}P < 0.01$ versus the control group. D-gal (L), low-dose D-gal group; D-gal (M), medium-dose D-gal group; D-gal (H), high-dose D-gal group.

probe was specific for the new fusion sequence, which was present only in mutant mtDNA that harbored the CD. As shown in Fig. 5, levels of the mtDNA CD were significantly higher in the D-gal-treated groups than that in the control group. In comparison with the control group, the accumulation of mtDNA CD in the low-dose, medium-dose and high-dose D-gal groups was increased by 1.70-fold, 2.41-fold, 3.67-fold, respectively ($P < 0.01$). These findings indicated that mtDNA damage was induced by D-gal in the VCN.

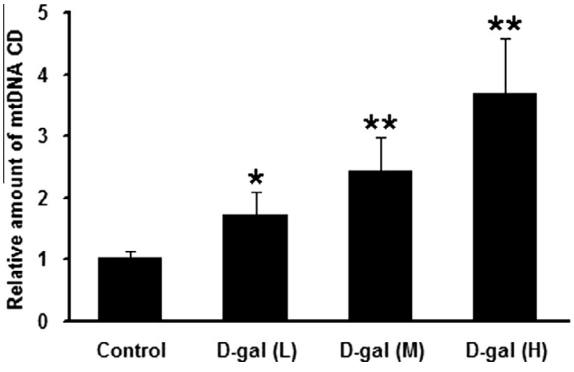

Fig. 5. Quantitative analysis of levels of the mtDNA CD in different groups. The level of the mtDNA common deletion was significantly increased in the D-gal-treated groups compared to the control group. All experiments were repeated three times. Data are expressed as mean ± SD of six rats per group. $^{*}P < 0.05$, $^{**}P < 0.01$ versus the control group. CD, common deletion; D-gal (L), low-dose D-gal group; D-gal (M), medium-dose D-gal group; D-gal (H), high-dose D-gal group; mtDNA, mitochondrial DNA.

Mitochondrial ultrastructural damage in the VCN induced by D-gal

To observe the changes to the mitochondrial ultrastructure induced by D-gal in the VCN, we compared the mitochondrial morphology between the D-gal-induced aging rats and control rats by TEM. As shown in Fig. 6, TEM revealed that the shape and size of mitochondria in the VCN of control rats were normal. In contrast, numerous mitochondria from the rats in the D-gal-treated groups were swollen with a reduced electron density in the matrix or serious degeneration. Additionally, lipofuscin granules frequently appeared in the cytoplasm of neurons in the VCN of rats in the high-dose D-gal group. These findings indicated that the mitochondrial ultrastructure was damaged by D-gal in the VCN.

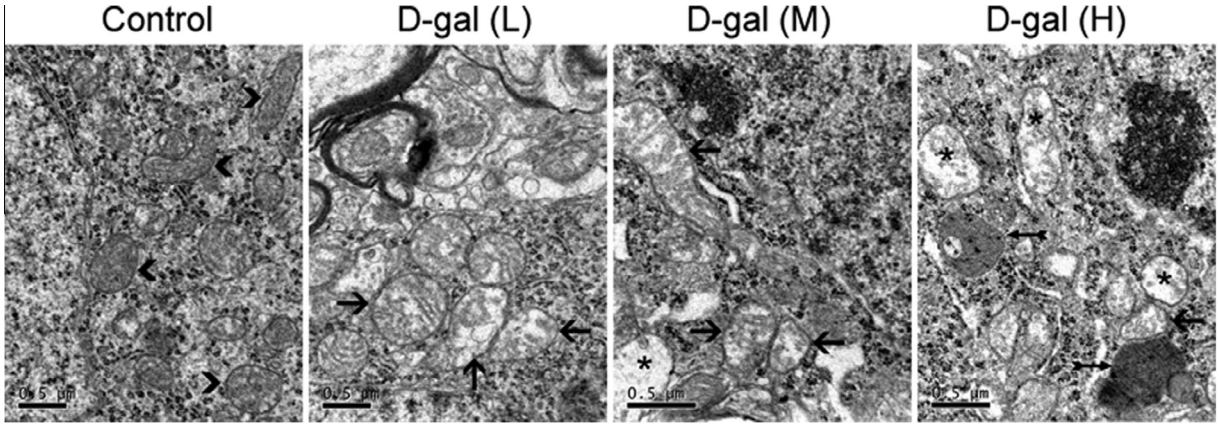

Fig. 6. Alterations in the mitochondrial ultrastructure in the VCN of rats in the D-gal-treated groups. Normal mitochondria (arrowheads) in the control group, swollen with a reduced electron density in the matrix of mitochondria (arrows) in the D-gal (L), D-gal (M) and D-gal (H) groups, the serious degeneration of mitochondria (asterisks) in the D-gal (M) and D-gal (H) groups, lipofuscin granules (double arrows) in the D-gal (H) group. $n = 4$ rats per group. Scale bar = 0.5 μm. D-gal (L), low-dose D-gal group; D-gal (M), medium-dose D-gal group; D-gal (H), high-dose D-gal group.

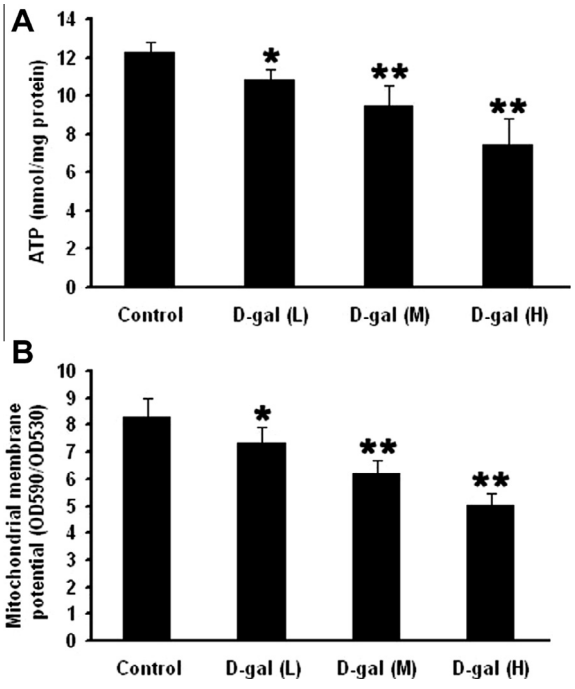

Fig. 7. Mitochondrial function in the VCN exposed to D-gal. (A) Levels of the ATP were significantly decreased in the D-gal-treated groups compared to the control group. (B) Levels of the MMP were also significantly decreased in the D-gal-treated groups compared to the control group. All experiments were repeated three times. Data are expressed as mean ± SD of six rats per group. $^{*}P < 0.05$ versus the control group; $^{**}P < 0.01$ versus the control group. D-gal (L), low-dose D-gal group; D-gal (M), medium-dose D-gal group; D-gal (H), high-dose D-gal group; MMP, mitochondrial membrane potential.

Mitochondrial dysfunction in the VCN induced by D-gal

To evaluate the mitochondrial function in the VCN, we measured the levels of ATP and MMP. As shown in Fig. 7A, B, the levels of ATP in the low-dose, medium-dose and high-dose groups of D-gal-treated rats were 10.73 ± 0.66 nmol/mg protein, 9.38 ± 1.14 nmol/mg protein, 7.39 ± 1.44 nmol/mg protein, respectively, which were significantly lower than those in the control groups (12.20 ± 0.59 nmol/mg protein) ($P < 0.05$ or $P < 0.01$); the levels of MMP in the low-dose, medium-dose and high-dose groups of D-gal-treated rats were 7.27 ± 0.62, 6.17 ± 0.50, 5.00 ± 0.44, respectively, which were significantly higher than those in the control groups (8.26 ± 0.72) ($P < 0.05$ or $P < 0.01$). These findings indicated that the mitochondrial function was damaged by D-gal in the VCN.

The mitochondrial apoptotic pathway in the VCN activated by D-gal

To investigate whether the mitochondrial apoptotic pathway was activated by D-gal in the VCN, the protein levels of cytosolic cyt c and cleaved caspase-3 were measured by western blot analysis and the apoptotic cells were detected by TUNEL staining. As shown in Fig. 8A–D, the protein levels of cytosolic cyt c and cleaved caspase-3 were significantly higher in the D-gal-treated groups than that in the control group. In comparison with the control group, cytosolic cyt c protein expression in the low-dose, medium-dose and high-dose D-gal groups was increased by 8.34-fold, 12.94-fold, 19.68-fold, respectively ($P < 0.01$); cleaved caspase-3 protein expression in the low-dose, medium-dose and high-dose D-gal groups was increased by 6.25-fold, 8.48-fold, 14.31-fold, respectively ($P < 0.01$). As shown in Fig. 9A, B, the TUNEL-positive cells in the low-dose, medium-dose and high-dose groups of D-gal-treated rats were 4.00 ± 0.41, 7.25 ± 0.48, 12.00 ± 0.91, respectively, which were also significantly increased compared with those in the control group (0.50 ± 0.29) ($P < 0.01$). These findings indicated that the mitochondrial apoptotic pathway was activated by D-gal in the VCN (Fig. 10).

DISCUSSION

In this study, we found that H_2O_2 and MDA increased and T-SOD activity decreased in the blood of D-gal-treated rats, which indicated that we could establish the animal

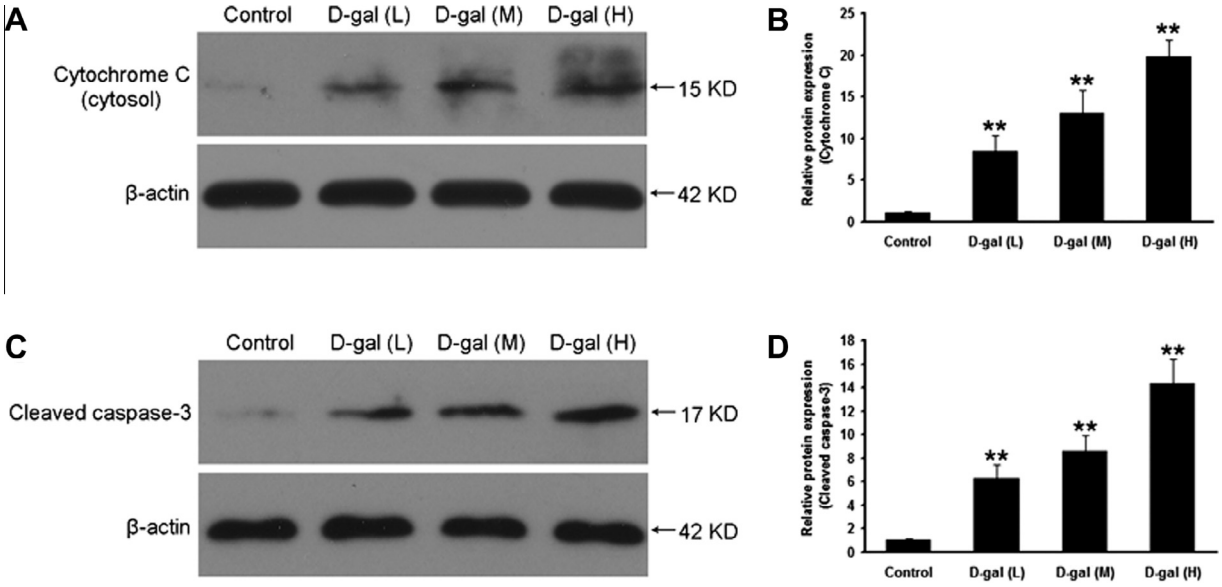

Fig. 8. Western blot and densitometric analysis of cytosolic cytochrome c and cleaved caspase-3 in the VCN. (A and C) Representative western blots showing the expression levels of cytosolic cytochrome c and cleaved caspase-3 in the different groups. (B and D) The relative abundances of the cytosolic cytochrome c and cleaved caspase-3 proteins were significantly increased in the D-gal-treated groups compared to the control group. All experiments were repeated three times. Data are expressed as mean ± SD of six rats per group. $^{**}P < 0.01$ versus the control group. D-gal (L), low-dose D-gal group; D-gal (M), medium-dose D-gal group; D-gal (H), high-dose D-gal group.

model of mimetic aging by D-gal (Ho et al., 2003). We also found that H_2O_2, one of the major types of ROS (Mates et al., 2012), significantly increased in the VCN of D-gal-treated rats, which also indicated that D-gal induced oxidative stress in the VCN. This study showed for the first time that NOX2 and its corresponding subunits $P22^{phox}$, $P47^{phox}$ and $P67^{phox}$ were significantly increased in the VCN of D-gal-treated rats, suggesting that D-gal might induce oxidative stress in the CAS via NOXs pathway and NOX2-dependent oxidative stress might play an essential role in the aging process of CAS. As opposed to mitochondria, which generate ROS as a byproduct of their metabolism, NOXs are professional ROS generators (Krause, 2007). The previous studies have demonstrated that NOX3 represents the primary source of ROS generation in the cochlea, which contributes to cisplatin-induced ROS production in the cochlea, while knockdown of NOX3 by siRNA can reduce NOX3-dependent ROS generation and against cisplatin-induced ototoxicity (Banfi et al., 2004; Mukherjea et al., 2010, 2011). The previous studies also indicated that NOX3-dependent ROS generation might be partially responsible for the degeneration in the PAS and NOX2-dependent oxidative stress might contribute to the mtDNA CD and mitochondrial ultrastructural damage in the hippocampus of D-gal-induced aging rats (Du et al., 2012a,b). Therefore, the over-expression of NOX2 might be also an important source of ROS in the aging process of CAS. Meanwhile, we also found that the over-expression of NOX2 correlated with increased 8-OHdG expression, a biomarker of DNA oxidative damage (Kujoth et al., 2005; Ma et al., 2011), in the VCN, suggesting that NOX2-dependent oxidative stress might be an important reason for the oxidative damage of DNA in the aging process of CAS.

Oxidative damage to mtDNA is the basis of Harman's free radical theory of aging (Harman, 2001). The mtDNA 4977-bp deletion (also known as the ''common deletion'', CD) in humans, and the corresponding mtDNA 4834-bp deletion in rats, is the most frequent aging-associated occurrence of mtDNA damage. Therefore, CD has been used as a biomarker for aging (Yowe and Ames, 1998; Nicklas et al., 2004; Meissner et al., 2008; Markaryan et al., 2009). An association between elevated mtDNA CD and presbycusis has been observed in a number of studies (Bai et al., 1997; Ueda et al., 1998; Meissner et al., 2008; Markaryan et al., 2009; Chen et al., 2010b). Although there was no significant difference in elevation of auditory brainstem response (ABR) threshold between the rats with mtDNA CD induced by D-gal and control rats, the hearing threshold in the rats carrying mtDNA CD increased significantly following aminoglycoside antibiotic injection compared to the control rats. These results indicated that the mtDNA CD may not directly lead to hearing loss, but rather act as a predisposing factor that can greatly enhance the sensitivity of the inner ear to aminoglycoside antibiotics (Kong et al., 2006). The previous studies have demonstrated that the accumulation of mtDNA CD increased in the PAS (Kong et al., 2006; Zhong et al., 2011a,b; Du et al., 2012b) and CAS (Chen et al., 2010a,b; Zhong et al., 2012) of D-gal-induced aging rats. In this study, we also found that the accumulation of mtDNA CD increased in the VCN of D-gal-treated rats and the increased accumulation of mtDNA CD correlated with DNA oxidative damage. To further evaluate mitochondrial damage in the VCN of D-gal-induced aging rats, we investigated changes in the mitochondrial ultrastructure by TEM. We observed that numerous mitochondria underwent degeneration in the VCN of D-gal-treated rats.

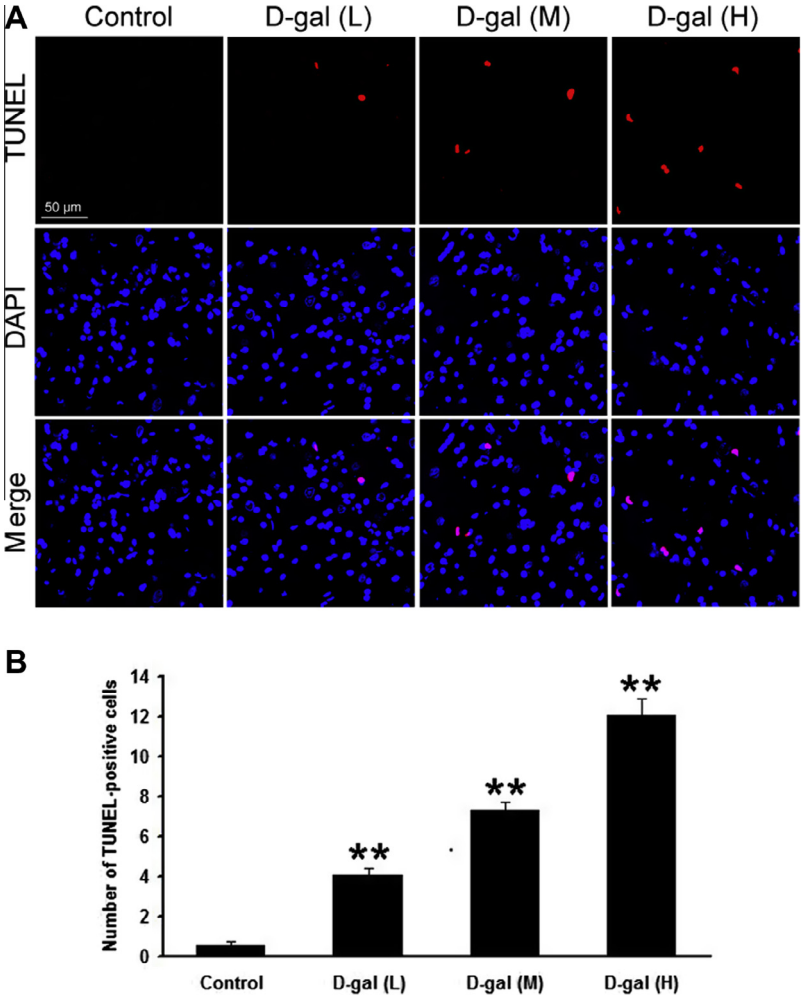

Fig. 9. Apoptotic cells in the VCN of rats in the different groups. (A) Representative images show apoptotic cells (red) in the VCN of rats in the different groups by TUNEL staining. Scalar bar = 50 μm. (B) Quantitative assessment of TUNEL-positive cells in the VCN. The TUNEL-positive cells in the VCN were significantly increased in D-gal-treated rats as compared with control rats. All experiments were repeated three times. Data are expressed as mean ± SD of four rats per group. $^{**}P < 0.01$ versus the control group. D-gal (L), low-dose D-gal group; D-gal (M), medium-dose D-gal group; D-gal (H), high-dose D-gal group. (For interpretation of the references to color in this figure legend, the reader is referred to the web version of this article.)

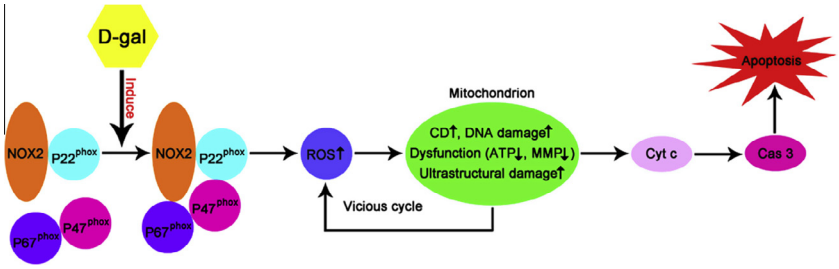

Fig. 10. Model of D-gal-induced oxidative stress and apoptosis in the VCN. D-Gal induces NOX2 and its corresponding subunits $P22^{phox}$, $P47^{phox}$ and $P67^{phox}$ form the active NOX2 enzyme complex to generate ROS, excess ROS impairs the mitochondrion and leads to the increase of mtDNA CD, mtDNA damage and the damage of mitochondrial ultrastructure and the decrease of mitochondrial function (ATP↓ and MMP↓), the impaired mitochondrion can also generate more ROS that increase the damage of the mitochondrion, this is a vicious cycle. At last, the impaired mitochondrion releases cyt c from the mitochondrial intermembrane space into the cytoplasm and triggers apoptosis via a caspase-3-dependent pathway. CD, common deletion; Cas3, caspase3; cyt c, cytochrome c; D-gal, D-galactose; MMP, mitochondrial membrane potential; mtDNA, mitochondrial DNA; NOX2, NADPH oxidase 2; ROS, reactive oxygen species; VCN, ventral cochlear nucleus.

Therefore, these findings suggest that mitochondrial damage in the VCN of D-gal-induced aging rats might be caused by oxidative damage.

The accumulation of mtDNA mutations and mitochondrial ultrastructure damage may lead to mitochondrial dysfunction and an energy deficiency. The

decline of ATP levels and the collapse of MMP may initiate apoptosis by releasing cyt c from the mitochondrial intermembrane space into the cytoplasm and trigger apoptosis via a caspase-3-dependent pathway (Hengartner, 2000; Green and Kroemer, 2004; Priyadarsini et al., 2010). The previous studies have demonstrated that apoptotic cells were increased in the CAS (Chen et al., 2010a,b) and caspase-3-dependent apoptotic pathway was activated in the PAS (Du et al., 2012b) of D-gal-induced aging rats. In the current study, the over-expression of cytosolic cyt c and cleaved caspase-3 and increased TUNEL-positive cells in the VCN of D-gal-induced aging rats indicated that the activation of caspase-3-dependent mitochondrial apoptotic pathway may be a central mechanism driving aging in the CAS.

CONCLUSION

The present findings indicate that a remarkable increase in NOX2 expression is involved in the accumulation of mtDNA mutations, the decline of ATP and MMP and the activation of caspase-3-dependent apoptosis in the CAS of D-gal-induced aging rats. NOX2 may be a useful therapeutic target to prevent or slow the development of presbycusis.

AUTHORS' ROLES

ZDD and CSG conceived and designed the experiments. ZDD, QY, LL, SL, JLZ, JH, CL and DQ performed the experiments. ZDD and QY analyzed the data. ZDD drafted the paper and CSG revised the grammar.

DISCLOSURES

None of the authors have any conflicts to disclose. All authors approved the final manuscript.

Acknowledgments—This work was supported by the Science and Technology Development Foundation of Shenzhen, China (No. JCYJ20140411092351692), the Medical Scientific Research Foundation of Guangdong Province, China (No. B2014370) and the Science and Technology Development Foundation of Shenzhen Nanshan District, China (No. 2012014).

REFERENCES

Bai U, Seidman MD, Hinojosa R, Quirk WS (1997) Mitochondrial DNA deletions associated with aging and possibly presbycusis: a human archival temporal bone study. Am J Otol 18:449–453.

Banfi B, Malgrange B, Knisz J, Steger K, Dubois-Dauphin M, Krause KH (2004) Nox3, a superoxide-generating NADPH oxidase of the inner ear. J Biol Chem 279:46065–46072.

Bedard K, Krause KH (2007) The Nox family of Ros-generating NADPH oxidases: physiology and pathophysiology. Physiol Rev 87:245–313.

Chen B, Zhong Y, Peng W, Sun Y, Hu YJ, Yang Y, Kong WJ (2010a) Increased mitochondrial DNA damage and decreased base excision repair in the auditory cortex of D-galactose-induced aging rats. Mol Biol Rep 38:3635–3642.

Chen B, Zhong Y, Peng W, Sun Y, Kong WJ (2010b) Age-related changes in the central auditory system: comparison of D-galactose-induced aging rats and naturally aging rats. Brain Res 1344:43–53.

Du Z, Hu Y, Yang Y, Sun Y, Zhang S, Zhou T, Zeng L, Zhang W, Huang X, Kong W, Zhang H (2012a) NADPH oxidase-dependent oxidative stress and mitochondrial damage in hippocampus of D-galactose-induced aging rats. J Huazhong Univ Sci Technol Med Sci 32:466–472.

Du Z, Yang Y, Hu Y, Sun Y, Zhang S, Peng W, Zhong Y, Huang X, Kong W (2012b) A long-term high-fat diet increases oxidative stress, mitochondrial damage and apoptosis in the inner ear of D-galactose-induced aging rats. Hear Res 287:15–24.

Frisina RD, Walton JP (2006) Age-related structural and functional changes in the cochlear nucleus. Hear Res 216–217:216–223.

Green DR, Kroemer G (2004) The pathophysiology of mitochondrial cell death. Science 305:626–629.

Hamilton ML, Van Remmen H, Drake JA, Yang H, Guo ZM, Kewitt K, Walter CA, Richardson A (2001) Does oxidative damage to DNA increase with age. Proc Natl Acad Sci USA 98:10469–10474.

Harman D (2001) Aging: overview. Ann N Y Acad Sci 928:1–21.

Hengartner MO (2000) The biochemistry of apoptosis. Nature 407:770–776.

Hiona A, Leeuwenburgh C (2008) The role of mitochondrial DNA mutations in aging and sarcopenia: implications for the mitochondrial vicious cycle theory of aging. Exp Gerontol 43:24–33.

Ho SC, Liu JH, Wu RY (2003) Establishment of the mimetic aging effect in mice caused by D-galactose. Biogerontology 4:15–18.

Howarth A, Shone GR (2006) Ageing and the auditory system. Postgrad Med J 82:166–171.

Kong WJ, Hu YJ, Wang Q, Wang Y, Han YC, Cheng HM, Kong W, Guan MX (2006) The effect of the MtDNA4834 deletion on hearing. Biochem Biophys Res Commun 344:425–430.

Krause KH (2007) Aging: a revisited theory based on free radicals generated by Nox family NADPH oxidases. Exp Gerontol 42:256–262.

Kujoth GC, Hiona A, Pugh TD, Someya S, Panzer K, Wohlgemuth SE, Hofer T, Seo AY, Sullivan R, Jobling WA, Morrow JD, Van Remmen H, Sedivy JM, Yamasoba T, Tanokura M, Weindruch R, Leeuwenburgh C, Prolla TA (2005) Mitochondrial DNA mutations, oxidative stress, and apoptosis in mammalian aging. Science 309:481–484.

Livak KJ, Schmittgen TD (2001) Analysis of relative gene expression data using real-time quantitative PCR and the 2(−Delta Delta C(T)) method. Methods 25:402–408.

Ma Y, Mehta SL, Lu B, Li PA (2011) Deficiency in the inner mitochondrial membrane peptidase 2-like (Immp21) gene increases ischemic brain damage and impairs mitochondrial function. Neurobiol Dis 44:270–276.

Markaryan A, Nelson EG, Hinojosa R (2009) Quantification of the mitochondrial DNA common deletion in presbycusis. Laryngoscope 119:1184–1189.

Mates JM, Segura JA, Alonso FJ, Marquez J (2012) Oxidative stress in apoptosis and cancer: an update. Arch Toxicol 86:1649–1665.

Meissner C, Bruse P, Mohamed SA, Schulz A, Warnk H, Storm T, Oehmichen M (2008) The 4977 bp deletion of mitochondrial DNA in human skeletal muscle, heart and different areas of the brain: a useful biomarker or more. Exp Gerontol 43:645–652.

Mukherjea D, Jajoo S, Kaur T, Sheehan KE, Ramkumar V, Rybak LP (2010) Transtympanic administration of short interfering (Si)RNA for the Nox3 isoform of NADPH oxidase protects against cisplatin-induced hearing loss in the rat. Antioxid Redox Signal 13:589–598.

Mukherjea D, Jajoo S, Sheehan K, Kaur T, Sheth S, Bunch J, Perro C, Rybak LP, Ramkumar V (2011) Nox3 NADPH oxidase couples transient receptor potential vanilloid 1 to signal transducer and activator of transcription 1-mediated inflammation and hearing loss. Antioxid Redox Signal 14:999–1010.

Nicklas JA, Brooks EM, Hunter TC, Single R, Branda RF (2004) Development of a quantitative PCR (TaqMan) assay for relative mitochondrial DNA copy number and the common mitochondrial DNA deletion in the rat. Environ Mol Mutagen 44:313–320.

Ozawa T (1997) Genetic and functional changes in mitochondria associated with aging. Physiol Rev 77:425–464.

Priyadarsini RV, Murugan RS, Sripriya P, Karunagaran D, Nagini S (2010) The neem limonoids azadirachtin and nimbolide induce cell cycle arrest and mitochondria-mediated apoptosis in human cervical cancer (Hela) cells. Free Radic Res 44:624–634.

Quinn MT, Ammons MC, Deleo FR (2006) The expanding role of NADPH oxidases in health and disease: no longer just agents of death and destruction. Clin Sci 111:1–20.

Serrano F, Kolluri NS, Wientjes FB, Card JP, Klann E (2003) NADPH oxidase immunoreactivity in the mouse brain. Brain Res 988:193–198.

Someya S, Yamasoba T, Kujoth GC, Pugh TD, Weindruch R, Tanokura M, Prolla TA (2008) The role of MTDNA mutations in the pathogenesis of age-related hearing loss in mice carrying a mutator DNA polymerase gamma. Neurobiol Aging 29:1080–1092.

Someya S, Yamasoba T, Weindruch R, Prolla TA, Tanokura M (2007) Caloric restriction suppresses apoptotic cell death in the mammalian cochlea and leads to prevention of presbycusis. Neurobiol Aging 28:1613–1622.

Ueda N, Oshima T, Ikeda K, Abe K, Aoki M, Takasaka T (1998) Mitochondrial DNA deletion is a predisposing cause for sensorineural hearing loss. Laryngoscope 108:580–584.

Youle RJ, Strasser A (2008) The Bcl-2 protein family: opposing activities that mediate cell death. Nat Rev Mol Cell Biol 9:47–59.

Yowe DL, Ames BN (1998) Quantitation of age-related mitochondrial dna deletions in rat tissues shows that their pattern of accumulation differs from that of humans. Gene 209:23–30.

Zhong Y, Hu Y, Peng W, Sun Y, Yang Y, Zhao X, Huang X, Zhang H, Kong W (2012) Age-related decline of the cytochrome c oxidase subunit expression in the auditory cortex of the mimetic aging rat model associated with the common deletion. Hear Res 294:40–48.

Zhong Y, Hu YJ, Chen B, Peng W, Sun Y, Yang Y, Zhao XY, Fan GR, Huang X, Kong WJ (2011a) Mitochondrial transcription factor a overexpression and base excision repair deficiency in the inner ear of rats with D-galactose-induced aging. FEBS J 278:2500–2510.

Zhong Y, Hu YJ, Yang Y, Peng W, Sun Y, Chen B, Huang X, Kong WJ (2011b) Contribution of common deletion to total deletion burden in mitochondrial DNA from inner ear of D-galactose-induced aging rats. Mutat Res 712:11–19.

(Accepted 20 November 2014)
(Available online 8 December 2014)